END EFFECTS IN MAGNETOHYDRODYNAMIC CHANNELS AT FINITE MAGNETIC REYNOLDS NUMBERS

V. F. Vasil'ev and I. V. Lavrent'ev

The effects of the magnetic Reynolds number have been examined via the distribution of the magnetic fields induced by the motion of a medium in a rectangular channel with conducting walls in the presence of an inhomogeneous magnetic field; the effects of wall conductivity and geometry of the external field are also examined as regards the distribution of the induced currents, the Joule loss, and the electric and magnetic fields over the cross section. The problem has previously been considered for a channel with insulating walls [1].

1. Consider a rectangular channel $|x| < \infty$, $|y| < a$ having thin conducting walls $y = \pm a$, in which there flows a liquid (conductivity σ) with a constant velocity $\mathbf{V} = (V, 0, 0)$ in the presence of an external magnetic field $\mathbf{B_e} = (0, 0, B_e(x))$. Currents are induced in the conducting medium, which produce a field $\mathbf{B_i}$ satisfying

$$\operatorname{rot} \mathbf{B}_i = \mu \mathbf{j}, \quad \mathbf{j}/\sigma = -\nabla\varphi + \mathbf{V} \times (\mathbf{B}_e + \mathbf{B}_i) \tag{1.1}$$

Here φ is the electrical potential in the channel, and $\mathbf{j}$ is the current density. We also assume that all quantities are independent of the z coordinate and that $j_Z = 0$; then (1.1) gives $\mathbf{B_i} = (0, 0, B_i(x,y))$. The basis for this assumption in an actual situation must be demonstrated in each particular case (see section 2). Then it follows from (1.1) that $B_i(x,y)$ should satisfy

$$\frac{\partial^2 B_i}{\partial x^2} + \frac{\partial^2 B_i}{\partial y^2} - \mu\sigma V \frac{\partial B_i}{\partial x} = \mu\sigma V \frac{\partial B_e}{\partial x} \tag{1.2}$$

The boundary conditions for $B_i(x,y)$ can be found via Shercliffe's boundary conditions [2] for the potential at the inside of a thin conducting wall

$$\frac{\partial\varphi}{\partial y} \pm \frac{\sigma_1 t}{\sigma} \frac{\partial^2\varphi}{\partial x^2} = V[B_e(x) + B_i(x)] \text{ for } y = \pm a \tag{1.3}$$

This gives, from (1.1) after integration with respect to x and use of $B_i = j_x = 0$ for $x = \pm\infty$, that the boundary condition for B_i is

$$B_i \pm \frac{\sigma_1 t}{\sigma} \frac{\partial B_i}{\partial y} = 0 \text{ for } y = \pm a \tag{1.4}$$

We use the dimensionless variables

$$x^\circ = x/a, \; y^\circ = y/a, \; j = \sigma V B j^\circ, \; \varphi = BVa\varphi^\circ$$
$$B_i = Bb(x^\circ, y^\circ), \; B_e = Bf(x^\circ)$$

and omit for simplicity the subscript zero in the dimensionless quantities to get the following boundary-value problem from (1.2) and (1.4):

$$\frac{\partial^2 b}{\partial x^2} + \frac{\partial^2 b}{\partial y^2} - R_m \frac{\partial b}{\partial x} = R_m \frac{\partial f}{\partial x} \qquad (R_m = \mu\sigma V a) \tag{1.5}$$

Leningrad. Translated from Zhurnal Prikladnoi Mekhaniki i Tekhnicheskoi Fiziki, No. 3, pp. 19-27, May-June, 1971. Original article submitted October 2, 1970.

$$b \pm d\frac{\partial b}{\partial y} = 0 \quad \text{for} \quad y = \pm 1 \qquad \left(d = \frac{\sigma_1 t}{\sigma a}\right)$$

$$\frac{\partial b}{\partial y} = 0 \quad \text{при } y = 0, |x| < \infty; \quad b \to 0 \quad \text{при } |x| \to \infty$$

Here B is some basis magnitude of the magnetic field, σ_1 and t are the conductivity and thickness of the wall, and R_m is the magnetic Reynolds number.

The solution to (1.5) can be constructed as a trigonometric series

$$b(x, y) = \sum_{n=1}^{\infty} A_n b_n(x) \cos \mu_n y \tag{1.6}$$

where the sum is taken over all nonnegative roots of

$$d\mu_n \operatorname{tg} \mu_n = 1 \tag{1.7}$$

where $\cos \mu_n y$ forms a complete system of functions orthogonal in the range $y \in [-1.1]$. Then (1.5) and (1.6) are used with the orthogonality of the $\cos \mu_n y$ to get

$$b_n(x) = e^{\gamma_+ x} \int_{\infty}^{x} \frac{df}{dx} e^{-\gamma_+ x} dx + e^{\gamma_- x} \int_{x}^{-\infty} \frac{df}{dx} e^{-\gamma_- x} dx \tag{1.8}$$

$$A_n = \frac{4R_m \sin \mu_n}{(2\mu_n + \sin 2\mu_n)\sqrt{R_m^2 + 4\mu_n^2}}, \quad 2\gamma_\pm = R_m \pm \sqrt{R_m^2 + 4\mu_n^2}$$

The above solution to (1.5) can be used to give the distribution of the electrical potential and the Joule heating. In (1.1) we put the potential as zero at $x = \pm\infty$, and integration with respect to x gives

$$\varphi(x, y) = -\frac{1}{R_m} \int_{\infty}^{x} \frac{\partial b(x, y)}{\partial y} dx \tag{1.9}$$

The Joule heat is determined as the work done by the Lorentz force in unit time*

$$Q = \int_{-\infty}^{\infty} dx \int_{-a}^{a} (\mathbf{B} \times \mathbf{j}) \mathbf{V} dy \tag{1.10}$$

We substitute (1.1) and (1.5) into (1.10) and integrate by parts to get an expression for the dimensionless Joule dissipation

$$q = \frac{Q}{\sigma E^2} = 8 \sum_{n=1}^{\infty} \frac{\sin^2 \mu_n}{\mu_n (2\mu_n + \sin 2\mu_n)(R_m^2 + 4\mu_n^2)^{1/2}} \int_{-\infty}^{\infty} \frac{df}{dx} b_n dx \tag{1.11}$$

$$E = 2BVa$$

2. A more or less realistic model is needed to establish the effects of R_m, σ_1, and the field distribution. Usually the pipe lies halfway between the poles of an electromagnet and the width of the pipe is substantially greater than the height. Also, we can assume closely that $\mathbf{B}_e = (B_{ex}(x, z), 0, B_{ez}(x, z))$ if the width of the poletips exceeds the pipe width by not less than the working gap.

Moreover, the z dependence of $\mathbf{B}_e$ can be neglected and one can assume $B_{ex} \approx 0$ if the pipe height is small relative to the gap. Then the distribution of the external magnetic field will correspond to that chosen in section 1.

It is far more complicated to consider the magnetic field of the induced currents. For the part of the pipe in the magnet we can assume that $\mathbf{B}_i$ is independent of z and that $B_{ix} = B_{iy} = 0$ if the poletips have infinite permeability. This is not obvious for the channel zone outside the magnet gap because the fields of the eddy currents at the inlet and outlet will be closed only partly through the iron, which makes B_{iz} dependent on y and z, while B_{ix} and B_{iy} cease to be zero.

*All quantities in (1.10) are dimensional.

This position becomes more difficult as R_m increases, particularly as regards the outlet; the induced magnetic field appears in the boundary conditions at the walls, and the problem becomes unclosed. The assumptions of section 1 and of (1.4) can be tested only by experiment or simulation, as an analytic solution is virtually impracticable.

The assumptions of section 1 and the solution apply when the walls perpendicular to the external magnetic field have ideal magnetic permeability or the poletips extend to infinity on both sides along the flow. We assume in future that this is so, but on the basis that the external magnetic field is specified by a relation that truly represents the distribution along the x axis.

Let the field be given in the form of [3]

$$f(x) = \begin{cases} 1 - A_1 \exp \nu_1 (|x| - c) & \text{for} \quad |x| < c \\ A_2 \exp \nu_2 (c - |x|) & \text{for} \quad |x| > c \end{cases} \tag{2.1}$$

The values

$$A_1 = 0.17, \quad A_2 = 0.83, \quad \nu_1 = 5.29 / 2\delta_*, \quad \nu_2 = 1.07 / 2\delta_*, \quad \delta_* = \delta / 2a, \quad c = \lambda / a$$

correspond to the real fall in the field.

Here δ is the pole gap and 2λ is the length of a poletip. Then (1.6), (1.8), and (2.1) give the distribution of the induced magnetic field as

$$b(x, y) = 4R_m \sum_{n=1}^{\infty} \frac{\sin \mu_n \cos \mu_n y b_n(x)}{(2\mu_n + \sin 2\mu_n)(R_m^2 + 4\mu_n^2)^{1/2}} \tag{2.2}$$

$$b_n(x) = \pm \frac{\nu_1 \nu_2 (R_m^2 + 4\mu_n^2)^{1/2} \exp [\pm \nu_2 (x \pm c)]}{(\nu_1 + \nu_2)(\nu_2 \mp \gamma_\mp)(\nu_2 \mp \gamma_\pm)} + \left[\frac{\nu_1 \nu_2 \exp (-\gamma_\pm c)}{(\nu_1 - \gamma_\pm)(\nu_2 + \gamma_\pm)} - \frac{\nu_1 \nu_2 \exp (\gamma_\pm c)}{(\nu_1 + \gamma_\pm)(\nu_2 - \gamma_\pm)} - \frac{2\nu_1 \nu_2 \gamma_\pm \exp (-\nu_1 c)}{(\nu_1 + \nu_2)(\nu_1^2 - \gamma_\pm^2)} \right] \exp \gamma_\pm x$$

Here the upper sign corresponds to $x \in (-\infty, -c]$, and the lower one to $x \in [c, \infty)$

$$b_n(x) = \pm \frac{\nu_1 \nu_2 (R_m^2 + 4\mu_n^2)^{1/2} \exp [\mp \nu_1 (x \pm c)]}{(\nu_1 + \nu_2)(\nu_1 \mp \gamma_-)(\nu_1 \pm \gamma_+)} \mp \frac{\nu_1 \nu_2 \exp [\gamma_\mp (x \pm c)]}{(\nu_1 \pm \gamma_\mp)(\nu_2 \mp \gamma_\mp)} \pm \left[\frac{\nu_1 \nu_2 \exp (\mp \gamma_\pm c)}{(\nu_1 \mp \gamma_\pm)(\nu_2 \pm \gamma_\pm)} \mp \frac{2\nu_1 \nu_2 \gamma_\pm \exp (-\nu_1 c)}{(\nu_1 + \nu_2)(\nu_1^2 - \gamma_\mp^2)} \right] \exp \gamma_\pm x$$

Here the upper sign corresponds to $x \in [-c, 0]$, and the lower one to $x \in [0, c]$.

Figure 1 shows the induced-current pattern for d = 1 and R_m of 0, 2, 10, and 50 as given by (2.2). Figure 1 shows that the eddy currents at the inlet and outlet for $R_m = 0$ are distributed symmetrically with respect to the center of the magnet. As R_m increases, the boundary to these currents moves along the direction of motion, and the inlet eddy begins to expand, its center shifting toward the middle of the magnet and attaining it for $R_m = \infty$. The outlet eddy also shifts down the flow as R_m increases and recedes to infinity as $R_m \to \infty$.

Formula (2.2) shows by direct integration that the total flux for the induced field is zero for all R_m and d, with the fluxes due to the live eddies equal in magnitude but opposite in sign; they increase with R_m and for $R_m = \infty$ become equal to the external flux, while the field of the outlet eddy and the total resultant field become zero. Figure 1 also shows that the lines of the induced field become straighter as R_m increases for a given d, and the induced field ceases to be dependent on y for $R_m = \infty$.

In (2.2) we let R_m tend to infinity and expand unity as a series in $\cos \mu_n y$:

$$1 = 4 \sum_{n=1}^{\infty} \frac{\sin \mu_n \cos \mu_n y}{2\mu_n + \sin 2\mu_n} \tag{2.3}$$

which allows us to show that the induced field becomes equal in magnitude and opposite in sign to the applied field, which is independent of y. A similar picture is seen as d increases for any R_m, which follows from (2.2); $d = \infty$ gives $\mu_n = \pi n$, $n = 0, 1, \ldots$, and all the terms vanish except that with $\mu_n = 0$, which makes the field independent of y.

Figure 2 shows the distribution of the resultant magnetic field $b_p = f + b$ at the middle of the pipe for c = 2 and $\delta_* = 0.75$ for various R_m and d. Curves 1(0), 2(1), 4(2), 6(5), 9(10), and 9(50) correspond to d = 0 while curves 10(1), 11(2), 12(5), 13(10), and 14(50) correspond to $d = \infty$, and curves 3(1), 5(1), and 7(1) correspond to d of 0.5, 1.0, and 5.0. The value of R_m is given in parentheses with each curve number.

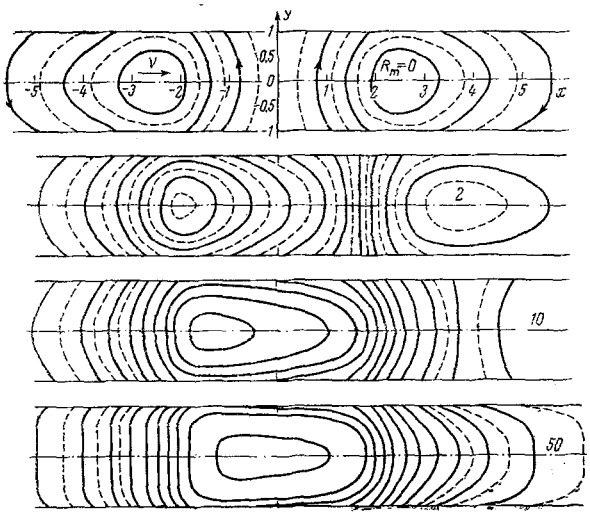

Fig. 1

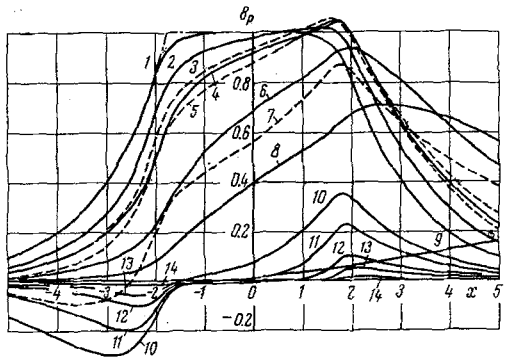

Fig. 2

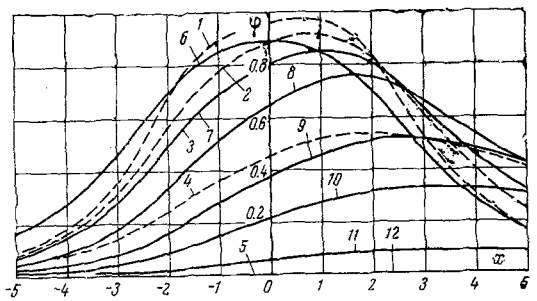

Fig. 3

The extent to which the field is carried down the flow direction increases with R_m; if d = 0, the field at the inlet is weakened while that at the outlet is strengthened. This tendency persists as d increases, with an overall reduction in the resultant magnetic field. (The field at the inlet becomes negative.) This reveals clearly the demagnetizing action of the induced currents; the resultant field near the poletips decreases as R_m increases and tends to zero as $R_m \to \infty$.

3. Consider $\varphi(x,y)$. We substitute (2.2) into (1.9) and get

$$\varphi(x, y) = 8 \sum_{n=1} \frac{\mu_n \sin \mu_n \sin \mu_n y}{(2\mu_n^2 + R_m \gamma_\pm)(2\mu_n + \sin 2\mu_n)} \left\{ \frac{\nu_1 \gamma_\pm (\gamma_- - \gamma_+) \exp \nu_2 (c \pm x)}{2(\nu_1 + \nu_2)(\nu_2 \mp \gamma_+)(\nu_2 \mp \gamma_-)} \pm \right.$$

$$\left. \pm \left[\frac{\nu_1 \nu_2 \gamma_\pm \exp(-\nu_1 c)}{(\nu_1 + \nu_2)(\nu_1^2 - \gamma_\pm^2)} + \frac{\nu_1 \nu_2 \operatorname{sh} \gamma_\pm c}{(\nu_1 \mp \gamma_\pm)(\nu_2 \pm \gamma_\pm)} + \frac{\gamma_\pm (\nu_1 - \nu_2) \nu_1 \nu_2 \exp(\pm \gamma_\pm c)}{(\nu_1^2 - \gamma_\pm^2)(\nu_2^2 - \gamma_\pm^2)} \right] \exp \gamma_\pm x \right\}$$

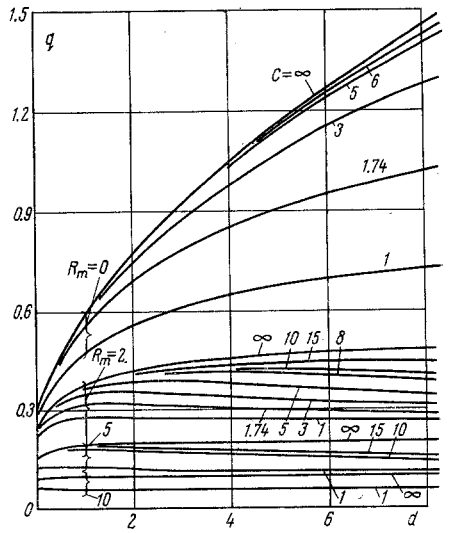

Fig. 4

The upper sign corresponds to $x \in (-\infty, -c)$, and the lower one to $x \in [c, \infty)$

$$\varphi(x, y) = 8 \sum_{n=1}^{\infty} \frac{\sin \mu_n \sin \mu_n y}{(4\mu_n^2 + R_m^2)^{1/2}(2\mu_n + \sin 2\mu_n)} \left\{ \frac{(4\mu_n^2 + R_m^2)^{1/2}}{2\mu_n} + \right.$$
$$+ \frac{\nu_1 \nu_2 \mu_n \exp \gamma_-(c + x)}{2\gamma_-(\nu_1 + \gamma_-)(\nu_2 - \gamma_-)} - \frac{\nu_1 \nu_2 \mu_n \exp \gamma_+(x - c)}{2\gamma_+(\nu_2 + \gamma_+)(\nu_1 - \gamma_+)} + \frac{\nu_2 \mu_n \exp(-\nu_1 c)}{\nu_1 + \nu_2} \times$$
$$\left. \times \left[\frac{\nu_1 \exp \gamma_\pm x}{\nu_1^2 - \gamma_\pm^2} + \frac{(4\mu_n^2 + R_m^2)^{1/2} \exp(\mp \nu_1 x)}{2(\nu_1 \pm \gamma_-)(\nu_1 \pm \gamma_+)} \right] \right\}$$

The upper sign corresponds to $x \in [-c, 0]$, and the lower one to $x \in [0, c]$.

Figure 3 shows the potential along the wall for c = 2 and $\delta_* = 0.75$ for various d and R_m. The curve numbers are from [3], with the corresponding d and R_m in parentheses: 1(0, 1), 2(0.5, 1), 3(1, 1), 4(5, 1), 5(∞, 1), 6 (1, 0), 7 (1, 1), 8(1, 2), 9(1, 5), 10(1, 10), 11(1, 50), 12(1, ∞). Consider the effects of R_m on the sensitivity $S = \varphi(0, 1)$, which characterizes the operation as a flowmeter. A fairly detailed discussion has been given [3] for the effects of δ_*, c, and d on the sensitivity.

The calculations show that, in the general case ($R_m \neq 0$), the qualitative arguments [3] on S remain correct here. Figure 3 shows that S and the maximum wall potential decrease as R_m increases, and the sensitivity may be increased by taking the signal from the wall at $(x_m, 1)$, where $x_m \geq 0$ and increases with R_m ($x_m = 0$ for $R_m = 0$).

4. Consider now the effects of R_m, σ_1, and field distribution on the Joule loss. The full expression is very inconvenient when the external field is defined by (2.1), and we give the simpler form

$$f_1(x) = \begin{cases} 1 & \text{for } |x| < c_1 \\ \exp \nu(c_1 - |x|) & \text{for } |x| > c_1 \end{cases} \qquad (4.1)$$

If c_1 is deduced from $f_1(c) = f(c)$ and we put $\nu = \nu_2$ [see (2.1)], calculation shows that the Joule losses differ by not more than 3% for external fields of (4.1) and (2.1). The broken line in Fig. 2 shows the field of (4.1) for $c_1 = 1.74$.

Then (4.1) gives the dimensionless Joule dissipation as

$$q = 2\nu^2 \sum_{n=1}^{\infty} \frac{\sin^2 \mu_n}{\mu_n(2\mu_n + \sin 2\mu_n)(\gamma_+ - \gamma_-)} \left[\frac{(\nu^2 - \mu_n^2)(2\nu + \gamma_- - \gamma_+) - \nu R_m^2}{\nu(\nu^2 - \gamma_-^2)(\nu^2 - \gamma_+^2)} - \frac{\exp(2\gamma_- c_1)}{(\nu - \gamma_-)^2} - \frac{\exp(-2\gamma_+ c_1)}{(\nu + \gamma_+)^2} \right] \qquad (4.2)$$

The dependence of q on ν^{-1} for the various R_m is as for $R_m = 0$ [3], i.e., the dissipation decreases as ν^{-1} increases ($q \to 0$ for $\nu \to 0$). Table 1 gives results from (4.2) for the dimensionless Joule loss for various R_m, d, and c_1 for the cases $\delta_* = 0$ in the first line ($\nu = \infty$, field given as a step) and $\delta_* = 0.75$ ($\nu = 0.714$) for the second.

In view of the above statement, for simplicity we consider only the case $\nu = \infty$, when (4.2) becomes

$$q = 2 \sum_{n=1}^{\infty} \frac{\sin^2 \mu_n [2 - \exp(2\gamma_- c_1) - \exp(-2\gamma_+ c_1)]}{\mu_n(2\mu_n + \sin 2\mu_n)(\gamma_+ - \gamma_-)} \qquad (4.3)$$

All subsequent conclusions from (4.3) are correct for all $\nu \neq \infty$, as one can see from Table 1.

Figure 4 shows q as a function of d, which characterizes the effects of wall conductivity, for various R_m and c_1 as deduced from (4.3). We see that R_m and wall conduction have different effects for $c_1 = \infty$, since $q \to 0$ as $1/R_m$ for $R_m \to \infty$, while increase in d causes q to increase monotonically and $q \to 1/R_m$ as $d \to \infty$, which follows from (4.3); the q(d) dependence becomes weaker as R_m increases, and q(d) attains its maximum value $q(\infty) = R_m^{-1}$ the earlier the larger R_m.

TABLE 1.

R_m	c	d = 0	d = 0.5	d = 1.0	d = 2.0	d = 5.0
0	1.0	0.2602	0.4001	0.4724	0.5563	0.6687
	1.0	0.0815	0.1717	0.2401	0.3429	0.5315
	1.74	0.2703	0.4415	0.5464	0.6843	0.8987
	1.74	0.0825	0.1783	0.2555	0.3781	0.6218
	8.0	0.2714	0.4520	0.5750	0.7626	1.1532
	8.0	0.0826	0.1800	0.2614	0.3996	0.7204
1.0	1.0	0.2451	0.3521	0.3929	0.4256	0.4450
	1.0	0.0778	0.1512	0.1940	0.2373	0.2652
	1.74	0.2568	0.3915	0.4518	0.5044	0.5336
	1.74	0.0794	0.1603	0.2120	0.2684	0.3085
	8.0	0.2591	0.4104	0.4973	0.6040	0.7270
	8.0	0.0797	0.1652	0.2276	0.3149	0.4341
2.0	1.0	0.2110	0.2670	0.2751	0.2735	0.2635
	1.0	0.0689	0.1134	0.1266	0.1279	0.1109
	1.74	0.2254	0.3003	0.3150	0.3114	0.2907
	1.74	0.0717	0.1252	0.1445	0.1500	0.1299
	8.0	0.2308	0.3322	0.3745	0.4081	0.4040
	8.0	0.0729	0.1369	0.1715	0.2099	0.2194
5.0	1.0	0.1216	0.1241	0.1181	0.1117	0.1056
	1.0	0.0411	0.0504	0.0409	0.0330	0.0233
	1.74	0.1352	0.1400	0.1316	0.1213	0.1105
	1.74	0.0463	0.0552	0.0502	0.0406	0.0278
	8.0	0.1493	0.1783	0.1787	0.1680	0.1427
	8.0	0.0516	0.0786	0.0850	0.0782	0.0569
10	1.0	0.0633	0.0594	0.0563	0.0537	0.0516
	1.0	0.0194	0.0172	0.0131	0.0096	0.0063
	1.74	0.0705	0.0654	0.0607	0.0565	0.0530
	1.74	0.0235	0.0208	0.0166	0.0120	0.0076
	8.0	0.0864	0.0895	0.0833	0.0741	0.0627
	8.0	0.0304	0.0387	0.0352	0.0277	0.0168
50	1.0	0.0117	0.0106	0.0103	0.0102	0.0101
	1.0	0.0019	0.0010	0.0007	0.0004	0.0003
	1.74	0.0125	0.0125	0.0106	0.0103	0.0101
	1.74	0.0024	0.0024	0.0009	0.0006	0.0003
	8.0	0.0158	0.0133	0.0122	0.0113	0.0106
	8.0	0.0052	0.0035	0.0024	0.0015	0.0008

However, q(d) becomes more complicated for finite c_1, and for $R_m \neq 0$ there is always a c_1 (which increases with R_m) q(d) has a maximum, with the corresponding d decreasing as R_m increases or as c_1 decreases. We shall see below that $q \to 0.5/R_m$ as $d \to \infty$ for $c_1 \neq \infty$.

This means that, in real cases, where the field size is always finite, one needs to be very careful in using formulas for the Joule loss derived for a semiinfinite field. One can neglect the interaction of the inlet and outlet currents for $c_1 > 2$ if $d = 0$ and $R_m = 0$, and the Joule loss can be determined as twice that for a semiinfinite field; but this cannot be done if R_m and d differ from zero, because the asymmetry in the resultant field becomes important, and the more so the greater R_m or d (see section 2). For instance, there is not more than 5% difference in the q between $c_1 = \infty$ and $c_1 = 1$ if $R_m = d = 0$, whereas $d = 0$ and $R_m = 50$ makes the Joule loss for $c_1 = \infty$ more than 1.5 times that for $c_1 = 1$ and more than twice that for $R_m = 0$ and $d = 10$.

Figure 4 shows that one can use the loss formula found for a semiinfinite field down to a lower limit in c_1 that increases with R_m and with d.

We derive an approximate formula for q before we consider the analytically similar behavior in relation to c_1, R_m, and d. From (2.3) with $y = 0$ and (4.3) we get

$$q = \frac{2 - \exp\left(R_m - \sqrt{R_m^2 + 4\mu_0^2}\right) c_1 - \exp\left(-R_m - \sqrt{R_m^2 + 4\mu_0^2}\right) c_1}{2\left(R_m^2 + 4\mu_0^2\right)^{1/2}} \tag{4.4}$$

The q of (4.3) and (4.4) differ by not more than 1% for R_m and $d > 1$, while (4.4) gives values slightly larger than those of (4.3) for R_m and $d < 1$. (The maximum difference is 14% for $R_m = d = 0$.) Figure 5 shows $\mu_0(d)$; (1.7) shows that $\mu_0^2 \approx d^{-1}$ for $d > 10$, in which case (4.4) gives, for R_m and c_1 such that $\exp(-2R_m c_1) \ll 1$,

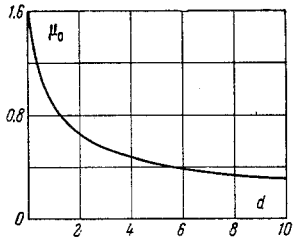

Fig. 5

$$q = \frac{2 - \exp(-2c_1 / R_m d)}{2[R_m^2 + (2/d)^2]^{1/2}} \qquad (4.5)$$

The exponential term contains all the c_1 dependence; if $c_1 = \infty$ for finite R_m and d, the numerator in (4.5) equals two, and $q \to 1/R_m$ for $d \to \infty$ and for finite R_m; if $c_1 \neq \infty$ and $d \to \infty$, $q \to 0.5/R_m$. From (4.5) we get the lower limit to c_1 for which one can use the formula for the Joule loss in the semiinfinite case, for which we must have

$$\exp(-2c_1 / R_m d) \ll 1$$

i.e., $2c_1 / R_m d$ must be greater than some number dependent on the required accuracy, so $c_1 > 0.5 A R_m d$.

Preliminary experiments and the results of [4] imply that the induced currents have less demagnetizing effect than the above theoretical analysis would imply, which occurs because (see section 2) the magnetic flux from the induced currents passes outside the magnetic circuit. Also, the solution takes no account of the shunting currents in the conducting walls or of the velocity profile in the pipe.

We are indebted to A. B. Vatazhin for his interest.

LITERATURE CITED

1. R. A. Boucher and D. B. Ames, "End effect losses in dc magnetohydrodynamic generators," J. Appl. Phys., 32, No. 5, 755-9 (1961).
2. J. Shercliffe, Theory of Electromagnetic Flow-Measurements, Cambridge University Press (1963).
3. V. F. Vasil'ev and I. V. Lavrent'ev, "A longitudinal boundary problem for the electric field in a MHD pipe with conducting walls," Mag. Gidr., No. 2 (1970).
4. G. A. Baranov, V. F. Vasil'ev, V. A. Glukhikh, B. G. Karasev, I. R. Kirillzhov, and I. V. Lavrent'ev, "Experimental studies of liquid-metal MHD generators," Electricity from MHD, Vol. 3, Vienna (1968).